

# The Importance of Intergalactic Structure to Gravitationally Lensed Quasars

R. Benton Metcalf<sup>1</sup>

*Department of Astronomy and Astrophysics, University of California, Santa Cruz, CA 95064 USA*

## ABSTRACT

Image flux ratio anomalies have been attributed to substructures within the gravitational lens and to small mass halos ( $M \lesssim 10^{10} M_{\odot}$ ) in intergalactic space. In this paper, analytic calculations are presented that help in the understanding of how intergalactic halos affect magnification ratios. It is found that intergalactic halos can produce anomalies at a similar level to those that are observed. Intergalactic halos with masses  $< 10^{10} M_{\odot}$  are expected to cause relative deflections between images of order 10 milliarcseconds, which are then magnified by the primary lens. They will also cause fluctuations in the surface density on the several percent level. The importance of intergalactic halos depends strongly on the radial profile of the halos and the primordial power spectrum at small scales. Strongly lensed quasars provide an opportunity to probe these properties. A strong dependence on the QSO redshift is predicted and can be used to distinguish between intergalactic structure and substructure as the cause of magnification anomalies. This analytic approach also explains why some previous semi-analytic estimates disagreed with numerical calculations.

## 1. Introduction

Gravitationally lensed quasars have recently been used to identify substructure in the dark matter halos of lens galaxies (Mao & Schneider 1998; Metcalf & Madau 2001; Metcalf & Zhao 2002; Metcalf 2002; Chiba 2002; Dalal & Kochanek 2002; Bradač et al. 2002; Keeton 2003; Metcalf et al. 2004). The Cold Dark Matter (CDM) model predicts a certain amount of small mass subhalos ( $\lesssim 10^7 M_{\odot}$ ) that do not have visible dwarf galaxy counterparts. These subhalos within the gravitational lens could be causing the observed anomalies in the image flux ratios, but it is also possible that they are being caused by clumps of matter somewhere along the line of sight, but not associated with the lens galaxies. Mao et al. (2004) have argued that  $\Lambda$ CDM does not predict enough substructure within galactic halos to account for the anomalies. Amara et al. (2004) have studied the lensing properties of lenses taken out of CDM simulations and found that they do not contain enough substructure, but this conclusion may be dependent on resolution. Future cosmological simulation with higher resolution might be able to verify this for certain.

It was found in Metcalf (2004), using numerical simulations, that intergalactic halos could account for most of the anomalies seen in the magnification ratios. This conclusion has been somewhat controversial largely because it disagrees with the conclusions of Chen, Kravtsov, & Keeton (2003) who found that the contribution from intergalactic halos would be  $\lesssim 10\%$  of that from substructure within the primary lens halo, not enough to account for the observed anomalies by themselves. Chen et al. (2003) relied on an analytic calculation where the deflection caused by the primary lens is approximated by a first order expansion and then the cross section as a function of magnification is calculated for a single perturbing substructure. In

---

<sup>1</sup>Hubble Fellow

this paper, it is demonstrated why this type of calculation is inadequate and how the results of the numerical simulations (Metcalf 2004) can be understood in terms of a simple analytic model.

This paper also makes clear what properties of small scale structure most affect the magnification ratios of strongly lensed quasars. Previously, the perturbing halos were simply modeled as truncated Singular Isothermal Spheres (SISs), except in Metcalf (2004), while here more realistic profiles are used and the sensitivity of lensing to their structure is investigated. The analytic model developed here demonstrates how flux ratio anomalies and Spectroscopic Gravitational Lensing (SGL) (see Metcalf et al. (2004)) can be used to study the small scale, or small mass, end of structure formation.

For the calculations in this paper the standard  $\Lambda$ CDM cosmological model is used with  $\Omega_m = 0.3$ ,  $\Omega_\Lambda = 0.7$ ,  $H_o = 70 \text{ km s}^{-1} \text{ Mpc}^{-1}$  and a scale free initial power spectrum. In the next section the density profiles and number densities of small mass dark matter halos are discussed. In section 3 the importance of intergalactic structure to the magnifications of QSO images is calculated both using a halo model, section 3.1, and directly from the power spectrum of density fluctuations, section 3.2. The conclusions are discussed in section 4.

## 2. Halo Profiles and Concentrations

From cosmological N-body simulations it has been found that the density profile of a dark matter halo tends to take a universal form given by (at least approximately) Navarro, Frenk & White (NFW) –  $\rho(r) = \frac{\delta_c \rho_c r_s}{r(1+r/r_s)^2}$  where  $\rho_c$  is the critical density of the universe and  $r_s$  is the scale size (Navarro, Frenk, & White 1997). The concentration of the halo is defined as  $c \equiv r_{200}/r_s$  where  $r_{200}$  is the radius within which the average density is 200 times the mean density of the universe, a proxy for the virial radius of the halo. The outer boundary of the halo is generally taken to be  $r_{200}$  as will be the case here. Once  $c$  and the mass,  $M$ , of a halo are fixed,  $\delta_c$  and  $r_s$  can be calculated. If a relationship between  $c$  and  $M$  is specified, the profile is a one parameter family.

The concentration increases with decreasing halo mass in the CDM model of structure formation. This is a result of smaller halos generally forming earlier, when the universe was denser. Navarro et al. (1997) propose a relation between concentration and mass by assuming that when a halo forms it contracts by a fixed factor from the mean density of the universe at that time. There is some ambiguity in defining the collapse time and not all halos of a given mass form at the same time so this prescription is at best approximate. More recently, fits to N-body simulations give approximately a power-law dependence of the concentration on subhalo mass,

$$c(M, z) = \frac{c_o}{(1+z)} \left( \frac{M}{10^{12} \text{ M}_\odot} \right)^\beta. \quad (1)$$

Values for  $\beta$  range from  $-0.1$  to  $-0.2$  and  $c_o \simeq 14$  (Bullock et al. 2001; Colín et al. 2004). In Metcalf (2004) a redshift independent  $c$ - $M$  relation was used as in Navarro et al. (1997). N-body simulations do show that the concentration of pure dark matter halos of a fixed mass should have a redshift dependence given above. This decreases their strength as lenses somewhat, as will be seen in section 3. However, there are a number of factors that complicate the  $c$ - $M$  relation and would be expected to increase the effective concentration of a halo.

In addition to dark matter, halos contain baryons that can significantly change their profiles. For example, the contraction of the baryons because of cooling and angular momentum loss will increase their density at the center of the halo and drag in additional dark matter, making

the profile steeper and more concentrated. Lensing results indicate that the inner regions of large galaxies have a profile that approximates a singular isothermal sphere (SIS),  $\rho(r) \propto r^{-2}$  (Treu & Koopmans 2004). These effects are expected to be smaller for small mass halos where the baryons do not cool efficiently and can be expelled by supernova feedback (Dekel & Silk 1986). Observed dwarf galaxies are known to have higher mass to light ratios than  $L_*$  galaxies (Mateo 1998; Kleyna et al. 2002). This also indicates that the profiles of small mass halos are more directly related to early structure formation driven by dark matter and less confused by feedback from star formation. With this in mind, it seems reasonable to approximate the profile of small mass halos by the NFW profile with a  $c$ - $M$  relation approximating (1), but, given the uncertainties and for the purposes of comparison with Metcalf (2004), a redshift independent  $c$ - $M$  relation will also be used in calculations.

The  $c$ - $M$  relation in N-body simulations also has a large scatter about the median (Bullock et al. (2001) find a  $1 \sigma$  scatter of  $\Delta(\log c) \simeq 0.2$ ). This is likely to increase the importance of these halos for lensing since their effects generally increase with concentration more rapidly than linear. This is another reason why expression (1) is a conservative approximation for our purposes.

The mass function of intergalactic halos is calculated using the Sheth-Tormen (Sheth & Tormen 2002) modification of the Press-Schechter (Press & Schechter 1974) method. This is known to agree with N-body simulations down to  $M \simeq 10^5 M_\odot$  (Colín et al. 2004). This prescription accounts only for isolated halos. All halos that have been resolved in N-body simulations contain substructure within them. This hierarchy of subhalos could conceivably increase the importance of intergalactic halos to lensing. This will not be taken into account in this paper.

### 3. Lensing by Intergalactic Halos

The situation of interest is one where a large primary lens that is creating multiple images of the QSO and additional small perturbing halos along the line of sight. First we will use the multiple lens planes approximation (see figure 1). Here the deflections caused by each object are treated as if they take place suddenly in the plane of the lens and the light follows an unperturbed geodesic between the planes. This is known to be a very good approximation. Given the angular position of a point on the source,  $\vec{\beta}$ , we must calculate the image points,  $\vec{\theta}$ , that correspond to it. If there are  $N$  lens planes these angular positions are related by

$$\vec{\phi}_{j+1} = \frac{D_{j+1}}{D_s} \vec{\theta} - \sum_{i=1}^j \frac{D_{i,j+1}}{D_s} \vec{\alpha}_i (D_s \vec{\phi}_i) \quad \vec{\beta} = \vec{\phi}_{N+1}(\vec{\theta}) \quad (2)$$

where  $D_i$  is the angular size distance to the  $i$ th lens,  $D_{i,j}$  is the distance between the  $i$ th and the  $j$ th lens planes and  $D_s = D_{N+1}$  is the distance to the source. The position in physical units on the  $i$ th lens plane is  $\vec{r}_i = D_s \vec{\phi}_i$  and the deflection angle caused by that lens is  $\vec{\alpha}_i(\vec{r}_i)$ . In general, the sub- or superscript  $l$  will refer to the primary lens. The distance to the primary lens is  $D_l$  and  $D_{l,N+1} = D_{l_s}$ . Equation (2) is only valid for a geometrically flat cosmology because it assumes that  $D_{i,i+1} + D_{i+1,i+2} = D_{i,i+2}$ . We assume that this is the case in this paper.

The magnification matrix is conveniently decomposed into the convergence,  $\kappa$ , and two components of shear,  $\gamma_1$  and  $\gamma_2$ ,

$$A_j^i(\vec{\theta}) \equiv \frac{\partial \beta^i}{\partial \theta^j} = \begin{pmatrix} 1 - \kappa - \gamma_1 & \gamma_2 \\ \gamma_2 & 1 - \kappa + \gamma_1 \end{pmatrix}. \quad (3)$$

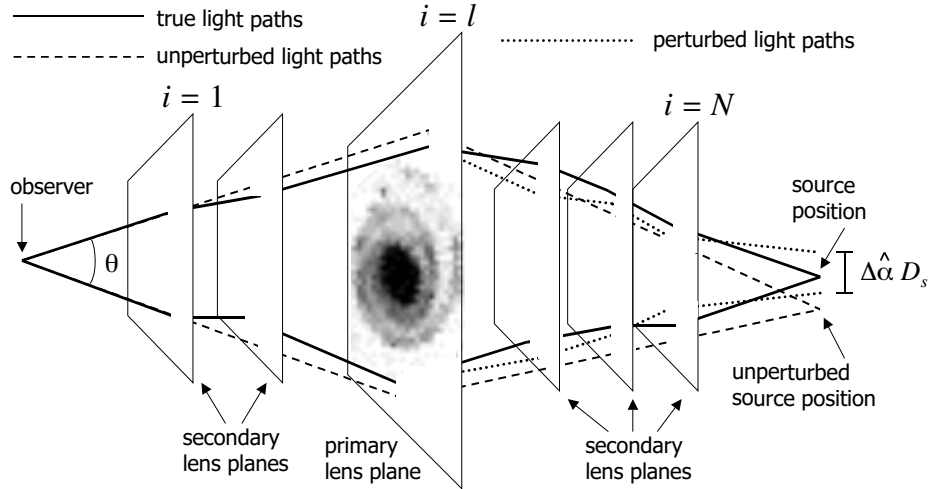


Fig. 1.— A schematic diagram of the type of lensing system being considered. There is one primary lens that is responsible for the multiple images of the source. In addition, there are many secondary lenses (most not shown). The two images represented here are separated by an angle  $\hat{\theta}$ . There may also be two other images that are not shown. The unperturbed light paths are deflected only by the primary lens and with an appropriate model for the primary lens will meet at the source plane. If the deflections from secondary lens planes are taken into account without changing the primary lens model the light will follow the perturbed light paths (dotted curves) and will not necessarily meet at a single source. On the source plane they will be separated by a distance  $\Delta\hat{\alpha} D_s$ . To get the true light paths the primary lens model needs to be adjusted so that they again meet at a single point on the source plane. The angle  $\Delta\hat{\alpha}$  is thus a measure of how wrong the lens model is when intergalactic lensing is not taken into account. This diagram is not to scale in any respect.

When there are multiple lens planes it is possible to get a rotation, but it will be small and of a higher order in the perturbations than is considered in this paper. In addition, rotation will not affect the magnification ratios. If there is only one lens plane, the convergence can be directly related to the local surface density,  $\kappa(\vec{r}_l) = \Sigma(\vec{r}_l)/\Sigma_{\text{crit}}$ . The critical surface density is  $\Sigma_{\text{crit}} = (4\pi G D_l D_{ls}/c^2 D_s)^{-1}$ . The magnification of a point-like image is  $\mu = (\det A)^{-1}$ .

### 3.1. simplified model

The influence of intergalactic halos on the magnification ratios and the cusp caustic relation was studied in Metcalf (2004) by directly solving equations (2) in numerical simulations. Numerical simulations are necessary for making accurate quantitative predictions, but a simplified model can help greatly with our understanding of which parameters and effects are important.

The essential difficulty with solving the lens equation (2) is that the positions on each lens plane are dependent on the positions on the other lens planes. The strategy taken here is to calculate quantities along unperturbed lines of sight, or the path the light would take if only the primary lens were present. For an unperturbed path, the position on the  $i$ th plane is

$$\vec{r}_i = D_i \vec{\theta} - \frac{D_i D_{ls}}{D_s} \begin{cases} \vec{\alpha}_i(D_l \vec{\theta}) & , \quad i > l \\ 0 & , \quad i \leq l \end{cases} \quad (4)$$

This approximation is valid as long as the deflections by intergalactic halos are small so that quantities that are second order in their deflections and derivatives of their deflections can be ignored.

The surface density of the NFW profile can be calculated directly, but the result is cumbersome. A simplified surface density can be used that exhibits the essential properties of the NFW profile and allows for some adjustments

$$\Sigma(r, z) = \frac{\Sigma_o}{(1 + r/r_s)^n} \quad (5)$$

where  $n \simeq 2$  is most like the NFW profile although  $n = 3$  will also be used to gain some insight into how the profile affects the lensing properties. For  $n = 2$  the mass within the radius  $r$  is

$$M(x) = 2\pi r_s^2 \Sigma_o \left[ \ln(1+x) - \frac{x}{1+x} \right] \quad x \equiv \frac{r}{r_s}. \quad (6)$$

The total mass is  $M_{200} = M(c)$  where the concentration,  $c(M_{200})$ , is given by (1). For  $n = 3$  a different expression for  $M(x)$  is derived, but  $M_{200}$  and  $c(M_{200})$  are defined in the same way.

Small halos affect the magnification of an image in two ways. One is from the halos changing the image positions and the primary lens' magnification being different at the new locations. Another way is for the substructure to contribute directly to the magnification of the image by changing  $A_j^i(\vec{\theta})$  without changing the image position enough to change the host lens's magnification. One of the goals of this paper is to determine which of these effects is more important. For this purpose the deflection, the convergence and the shear along the unperturbed path will be considered separately in the next two subsections.

### 3.1.1. deflection

The deflection angle caused by a axisymmetric halo is

$$\vec{\alpha}(\vec{r}) = 4GM(r/r_s) \frac{\vec{r}}{r^2}. \quad (7)$$

From the lens equation (2) it is seen that the important quantity is  $\hat{\alpha}(r) = \frac{D(z_s, z_s)}{D_s} \vec{\alpha}(r)$  which is the lowest order displacement of a light ray on the source plane (see figure 1).

Since  $|\alpha(r)|$  falls only as  $r^{-1}$ , for large  $r$  it might be expected that the deflections of many halos will add up to a total that is substantially larger than what an individual halo is likely to cause by itself. In fact,  $\langle \hat{\alpha}(\theta)^2 \rangle$  diverges logarithmically in the plane lens approximation because the number of halos rises as  $r^2$ . This is not a problem here however because only differences in the deflection angle are important. A constant deflection over the entire lens is equivalent to a shift in the position of the source. Such a uniform shift would be taken into account when fitting

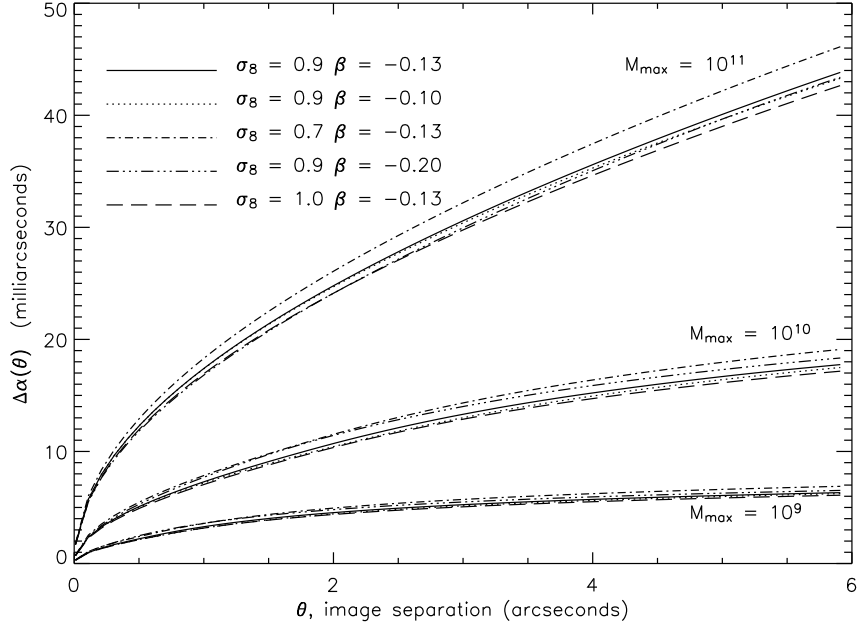


Fig. 2.— The root-mean-squared perturbation to the angular separation,  $\Delta\hat{\alpha}(\theta)$ , as a function of images separation,  $\theta$ . The range of halo masses included is  $10^4 M_\odot < M < 10^{11} M_\odot$  for the upper set of curves,  $10^4 M_\odot < M < 10^{10} M_\odot$  for the middle set and  $10^4 M_\odot < M < 10^9 M_\odot$  for the lowest set. In each set there are curves with varying values for the power spectrum normalization,  $\sigma_8$ , and the dependence of concentration on halo mass,  $\beta$ .

a primary lens model so it cannot produce any anomaly in the magnification ratios. However, if the deflections are different for the different images then they will cause the image positions to shift independently.

To assess the significance of these deflections we calculate the correlation function between the perturbations to the deflection caused by intergalactic halos as a function of the image separation. The positions of the halos will be treated as random and uncorrelated. In this case the correlation is

$$\Delta\hat{\alpha}(\theta)^2 \equiv \left\langle \left[ \hat{\alpha}(\vec{\theta}') - \hat{\alpha}(\vec{\theta}' + \vec{\theta}) \right]^2 \right\rangle \quad (8)$$

$$= \frac{1}{H_o D_s^2} \int_0^{z_s} dz \frac{D(z, z_s)^2}{\sqrt{\Omega(1+z)^3 + \Omega_\Lambda}} \int_0^{M_{\max}} dM \frac{dN}{dM}(M, z) \times \int d^2 r |\vec{\alpha}(\vec{r}) - \vec{\alpha}(\vec{r} + \vec{y}(z, \theta))|^2 \quad (9)$$

where  $\vec{y}(z, \theta)$  is the physical separation of two unperturbed lines of sight given by (4). These integrals are calculated numerically. The range of the  $r$  integral in (9) is increased until the answer stops changing.

Figure 2 shows  $\Delta\hat{\alpha}(\theta)$  for a source at  $z_s = 3$  and lens at  $z_l = 0.5$ . The most important parameter for  $\Delta\hat{\alpha}(\theta)$  is the upper halo mass cutoff,  $M_{\max}$ . The concentration and  $\sigma_8$  are relatively unimportant. Using a redshift independent  $c$ - $M$  relation gives slightly larger values for  $\Delta\hat{\alpha}(\theta)$ , but it is much smaller than the dependence on  $M_{\max}$ . Figure 3 what redshifts are

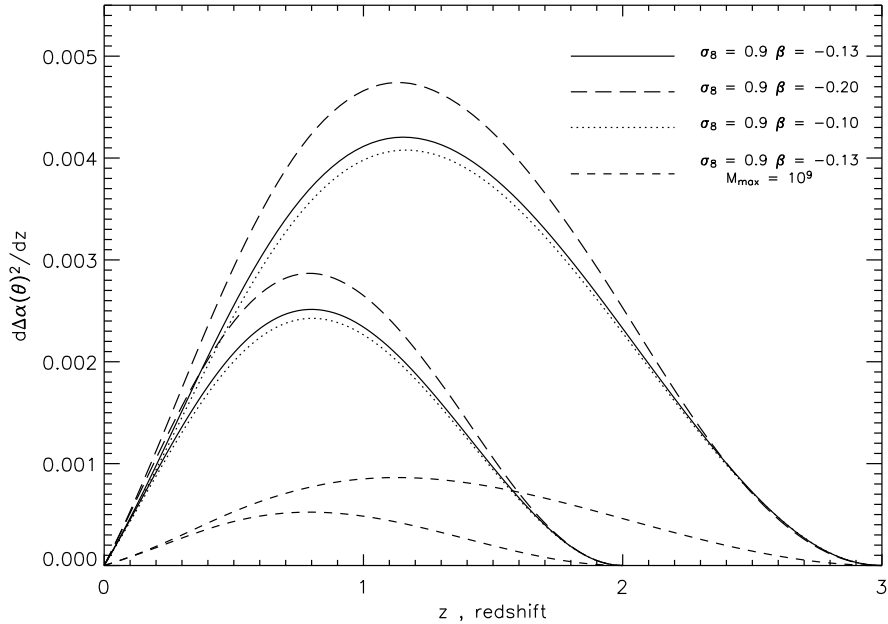


Fig. 3.— The contribution to  $\Delta\hat{\alpha}(\theta)^2$  from intergalactic halos as a function of redshift. The curves that end at  $z = 3$  are for a source at that redshift and a primary lens at  $z_l = 0.5$ . For the others  $z_s = 2$  and  $z_l = 0.3$ . The halo mass range is  $10^4 M_\odot < M < 10^{10} M_\odot$  in all cases except for the short dashed curves where  $10^4 M_\odot < M < 10^9 M_\odot$ . The image separation is set to 1 arcsecond.

contributing to  $\Delta\hat{\alpha}(\theta)$ . For a QSO at  $z = 3$  the majority of the deflection is coming from halos above  $z = 1$ .

The deflections shown in figure 2 can have a significant effect on the image magnifications even if the convergence and shear caused by the substructures are small. This is because, for a single image, the perturbation to the deflection acts like a *local* change in the source position. The change in the local source position can be magnified by the host lens to resulting in a substantial change in the image position. Even if the intergalactic halos did not affect the local magnification as a function of image position they would affect where the images form and thus change the magnification caused by the primary lens. This is an effect that is completely absent from a cross section type calculation where the host lens' deflection is expanded to first order (constant magnification). Local changes in the source position on the order of 15 milliarcseconds do cause changes in the magnification ratios even in Einstein cross type lenses. However, as will be shown in section 3.1.2, the intergalactic halos will modify the magnification directly as well and probably this second effect is more important.

The clustering of the halos has not been taken into account in this calculation. Clustering into filaments and other structures will only increase the value of  $\Delta\hat{\alpha}(\theta)^2$ . Because the deflection caused by a halo has such a long range the increase in  $\Delta\hat{\alpha}(\theta)^2$  could be significant, but it will not be investigated here.

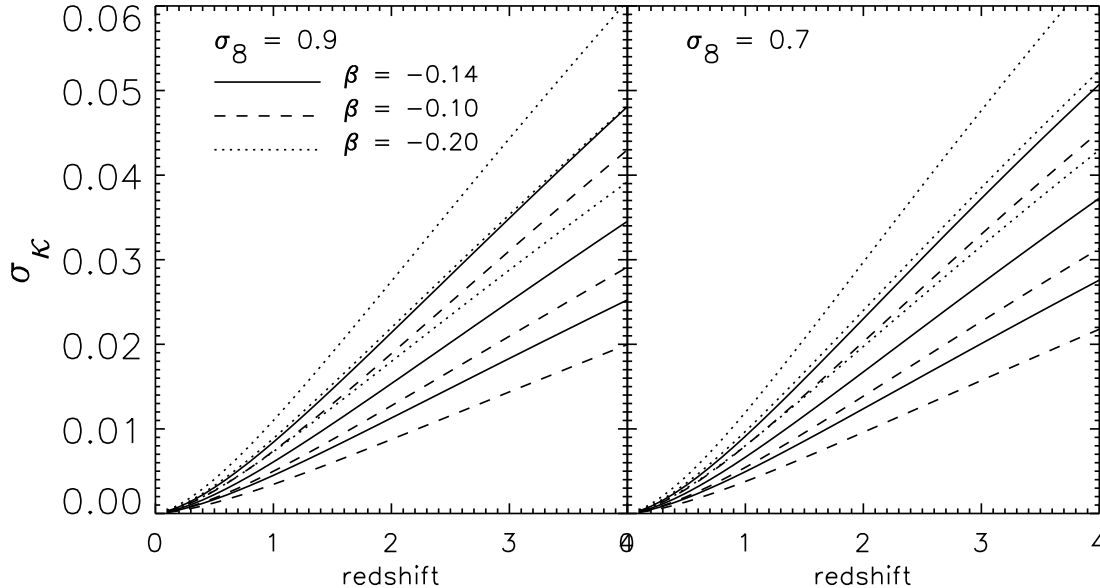


Fig. 4.— The standard deviation in the dimensionless surface density in small scale structure along random lines of sight as a function of source redshift. For the right panel the power spectrum normalization is  $\sigma_8 = 0.9$  as measured by (Spergel et al. 2003) and on the left a lower normalization is used  $\sigma_8 = 0.7$ . The halo mass-concentration relation is specified by the  $\beta$  values for each type of curve. For each set of like curves the upper one is for a halo mass range of  $10^3 M_\odot < M < 10^{11} M_\odot$ , the middle one is for  $10^3 M_\odot < M < 10^{10} M_\odot$  and the lower one is for  $10^3 M_\odot < M < 10^9 M_\odot$ .

### 3.1.2. convergence & shear

By taking an unperturbed light path in the lens equation (2) and then calculating its derivatives it is easily shown that, to lowest order, the total convergence,  $\kappa$ , is the sum of all the surface densities of all the halos along the line of sight weighted by the critical density,

$$\kappa(\theta) \simeq \sum_i \frac{\Sigma_i(\vec{\theta})}{\Sigma_{\text{crit}}(z_i, z_s)} = \sum_i \kappa_i(\vec{\theta}). \quad (10)$$

In the standard halo model of structure in the universe, all mass is in halos of some size. The standard expression for the angular size distance in a homogeneous universe takes into account the average surface density so, what is important for perturbations in the image magnifications is the variation in  $\kappa(\vec{\theta})$  about the mean. In addition, if the perturbation is uniform over the entire lens area, it will not affect any observables because of the mass sheet degeneracy. To cause anomalies in the magnification ratios  $\kappa(\theta)$  must have significant fluctuations on a scale that is smaller than roughly the Einstein ring radius of the primary lens ( $\sim 1$  arcsecond).

From the halo profile and the mass function the variance in  $\kappa$  along an unperturbed line of sight,  $\sigma_\kappa^2 \equiv \langle \kappa^2 \rangle - \langle \kappa \rangle^2$ , can be calculated assuming uncorrelated halo positions in the same



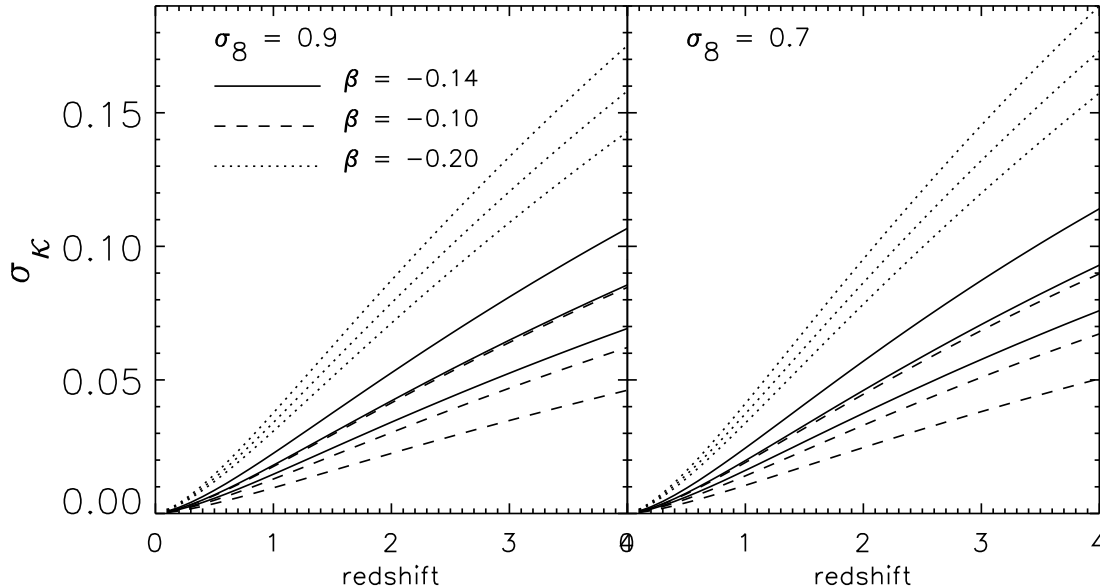


Fig. 5.— The standard deviation in the dimensionless surface density in small scale structure. Everything is the same as in figure 4 except that the halo profile is modified so that it is cutoff more sharply,  $n = 3$  in equation (5). The variance is significantly larger.

manner as the deflection angle was calculated in section 3.1.1,

$$\sigma_{\kappa}^2(\theta) = \frac{1}{H_o} \int_0^{z_s} dz \frac{\Sigma_{\text{crit}}(z, z_s)^{-2}}{\sqrt{\Omega(1+z)^3 + \Omega_{\Lambda}}} \int_0^{M_{\text{max}}} dM \frac{dN}{dM}(M, z) \quad (11)$$

$$\times \int_0^{\infty} d^2r \Sigma(\vec{r}, M, z) \Sigma(\vec{r} + \vec{y}(z, \theta), M, z)$$

The mass integral is bounded on the top by the minimum mass of a halo that one would expect to have an observable galaxy inside it. Any observed galaxies would be included in the primary lens model.

Figure 4 shows the result for  $\sigma_{\kappa}(0)$  as a function of source redshift. It can immediately be seen that the contribution of intergalactic halos to millilensing can be significant. Previous estimates for the amount of substructure required to account for the monochromatic magnification anomalies were a few percent. Given that the surface density in the primary lens is  $\kappa \simeq 0.5$  at the critical curve near where the images are located, the surface densities in figure 4 are substantial. Just like for  $\Delta\hat{\alpha}(\theta)$ ,  $\sigma_{\kappa}(\theta)$  will only increase when the clustering of the halos is included.

By comparing figures 4 and 2, it is seen that  $\sigma_{\kappa}(\theta)$  has a stronger dependence on smaller mass halos, while  $\Delta\hat{\alpha}(\theta)$  is heavily weighted toward the high end of the mass range. One can also see in figure 4 that the concentration of these halos has an important influence on their lensing properties. The redshift dependence is also important. A way to distinguish intergalactic halos from substructure in the primary lens is to measure how the anomalies depend on source

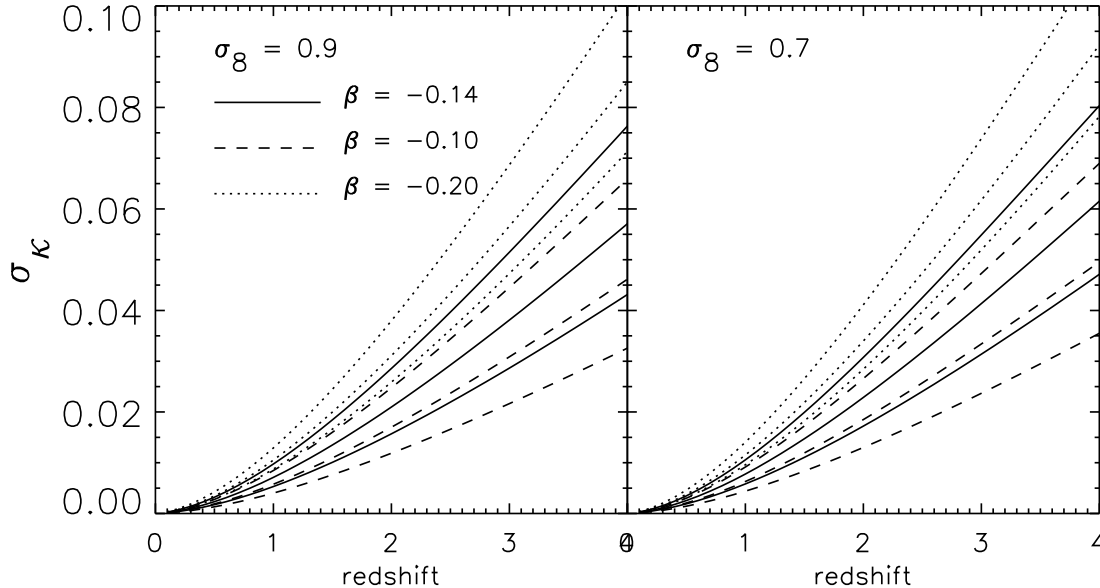


Fig. 6.— The standard deviation in the dimensionless surface density in small scale structure. Everything is the same as in figure 4 except that the mass–concentration relation is given by equation (1) without the redshift dependence and with  $c_o = 12$ . The redshift dependence tends to reduce  $\sigma_\kappa$  somewhat.

redshift. Since the space density of small scale halos becomes larger at higher redshift there is a significant increase in  $\sigma_\kappa(z)$  over the range of observed QSOs lenses ( $z \sim 1$  to 4). The dependence of the normalization of the matter power spectrum may be counter intuitive to some. If  $\sigma_8$  is reduced, more of the mass is in smaller halos and since we are only including small halos (well below  $M_*$ , the nonlinear mass scale),  $\sigma_\kappa$  is increased. If the current measurements of  $\sigma_8$  are taken into consideration and the primordial power spectrum is assumed to be scale invariant down to these scales, this effect is relatively small compared with the importance of halo concentration. If scale invariance is broken however this could become an important dependency.

A very interesting and illuminating thing occurs when  $n \neq 2$ . Figure 5 shows the same quantities as in figure 4 only with the large  $r$  slope changed to  $n = 3$ . This has the effect of cutting the halos off more abruptly and, to conserve mass, increasing their central densities. It is clearly seen that  $\sigma_\kappa$  is larger in this case. This strong dependence on  $n$  demonstrates that it is not the inner core of a single halo that is doing most of the lensing, as is implicitly assumed in a cross section type calculation. The important property is the profile at radii where the halos are likely to overlap on the sky. A cross section type calculation does not account for this since there the line of sight is assumed to intersect with at most one halo.

Figure 6 shows  $\sigma_\kappa(z)$  with a redshift independent  $c$ - $M$  relation. The same  $c$ - $M$  relation was used in the simulations of Metcalf (2004). The fluctuations in  $\kappa$  are similar, but larger in this case. It is possible that baryonic contraction in the larger halos could convert the inner region of their profiles into the SIS form ( $\rho(r) \propto r^{-2}$ ) at some high redshift. If this is the case,  $\sigma_\kappa(z)$

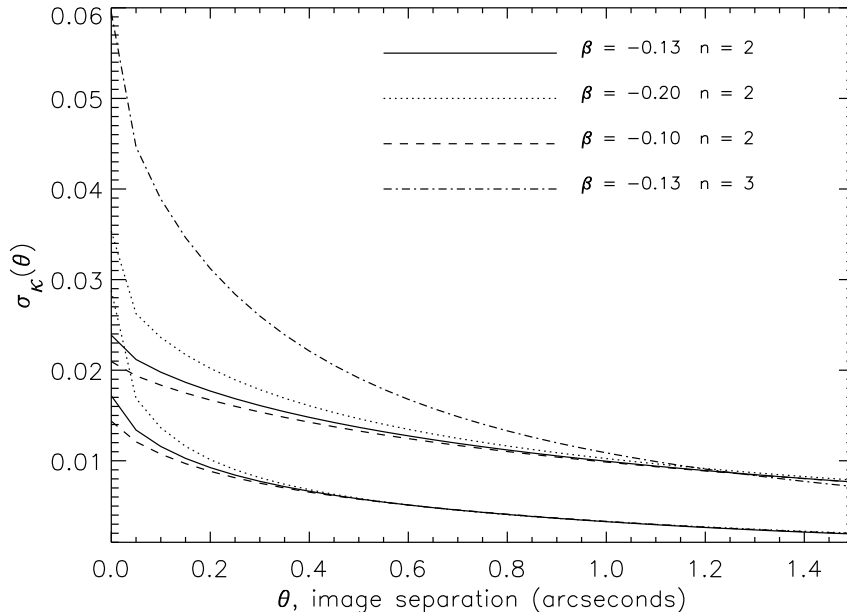


Fig. 7.— The correlation of surface density as a function of angular separation between images. The values for the halo parameters  $\beta$  and  $n$  are listed. The three lowest curves (for most of the  $\theta$ -range) are for halo mass ranges  $10^3 M_\odot < M < 10^9 M_\odot$  and the others are for  $10^3 M_\odot < M < 10^{10} M_\odot$ . The source is taken to be at  $z_s = 3$  and the primary lens is at  $z_l = 0.5$ . The power spectrum normalization is  $\sigma_8 = 0.9$  in all cases. Only one  $n = 3$  curve is included for clarity of the plot.

will be even larger. If the  $z = 0$  normalization can be established by other means, the redshift dependence of the magnification ratio anomalies can be used to measure the redshift dependence of the  $c$ - $M$  relation.

As mentioned before, if the fluctuations in  $\kappa(\theta)$  have a coherence length that is much larger than the size of the primary lens, they will have no observable effects because of the mass sheet degeneracy. Figure 7 shows  $\sigma_\kappa(\theta)$  as a function of image separation. Most of the fluctuations caused by halos of mass  $< 10^{10} M_\odot$  are on a significantly smaller scale than typical image separations. The concentrations of the halos appear to strongly affect only the small scale fluctuations below a few tenths of an arcsecond.

One might be concerned that the variance in  $\kappa(\vec{\theta})$  is not a good quantity for evaluating variations. Often, distributions in lensing have long tails which make the variance misleadingly large – for example the distribution of microlensing magnification caused by point masses. This is not the case here because the halo profile used does not diverge at the center or fall off too slowly at large  $r$ . This makes  $\sigma_\kappa$  a trustworthy indicator of typical variations. It is possible that the halos are highly clustered which would make  $\sigma_\kappa$  larger and skew the distribution so that the mode lies below the mean. If this were a dramatic effect the standard expression for the angular size distance would not apply to most high redshift objects.

The variance in the shear along random lines of sight, defined as  $\sigma_\gamma^2 = \langle \gamma_1^2 + \gamma_2^2 \rangle$ , can be calculated in the same way as  $\sigma_\kappa^2$  was calculated. However, the requirement that the distribution of halo positions be isotropic automatically guarantees that  $\sigma_\gamma^2(\theta) = \sigma_\kappa^2(\theta)$ . This is best demonstrated in Fourier space so the explanation will be deferred until section 3.2. Despite this,

an explicit calculation of  $\sigma_\gamma^2(0)$  has been done with the halo model and it is found to equal  $\sigma_\kappa^2(0)$  to very high accuracy which provides a reassuring consistency check.

The perturbations to the magnification matrix represented in figure 4 are on the several percent level. It might seem like this is too small to be of importance, but in fact these perturbations can strongly affect the magnifications of the images. To see this, the magnification can be expanded around the value for the primary lens alone,  $\mu_l$ ,<sup>2</sup>

$$\frac{\Delta\mu}{\mu_l} \simeq 2\mu_l [(1 - \kappa_l)\delta\kappa + \vec{\gamma}_l \cdot \delta\vec{\gamma}]. \quad (12)$$

The variance in the perturbation to the magnification is

$$\left(\frac{\Delta\mu}{\mu_l}\right)_{\text{rms}} \simeq 2\mu_l\sigma_\kappa(0)\sqrt{(1 - \kappa_l)^2 + \frac{\gamma_l^2}{2}} \quad (13)$$

where the fact that  $\sigma_\gamma^2(\theta) = \sigma_\kappa^2(\theta)$  has been used. Galactic sized lenses are well fit by singular isothermal ellipsoid (SIE) models, in which case the images form at  $\kappa_l \approx \gamma_l \approx 0.5$ . In this case  $\left(\frac{\Delta\mu}{\mu_l}\right)_{\text{rms}} \approx \mu_l\sigma_\kappa$ . For an image with a modest magnification of 5 this will exceed 10% if the source is at  $z_s \gtrsim 2$ . For more highly magnified images and/or higher redshift sources this can be significantly larger. And if halos have a steeper cutoff than NFW at large  $r$  it can be much larger. The level of the observed anomalies is on the  $\sim 10\%$  level (Metcalf & Zhao 2002). And direct numerical simulations give similar results (Metcalf 2004).

### 3.2. power spectrum approach

The second order statistics calculated thus far using the halo model can also be calculated in terms of the power spectrum of density fluctuations. This may be a more direct, although somewhat more obscure, way of interpreting the observations since the halo model contains more information than do  $\sigma_\kappa^2(\theta)$  or  $\Delta\hat{\alpha}(\theta)^2$ . The power spectrum also has the advantage of including within it the correlations in halo positions which were ignored in the previous section and it can be calculated relatively easily from a N-body simulations. With enough data one could think of inverting the variance in magnification anomalies to get a constraint on the power spectrum at small scales.

The deflection along a short section of the light path is

$$\vec{\alpha}(\vec{\theta}) = 2\vec{\nabla}_\perp \Phi(\vec{x}(\vec{\theta}, z)) \delta l \quad (14)$$

where  $\Phi(\vec{x})$  is the Newtonian potential,  $\vec{\nabla}_\perp$  is the gradient operator in the two dimensions perpendicular to the light path and  $\delta l$  is the path length. If the unperturbed path is substituted in for  $\vec{x}(\vec{\theta}, z)$ , the potential is Fourier transformed, and all the deflections along the path are added up one gets

$$\hat{\alpha}(\vec{\theta}) = (8\pi G\rho_o) \int dR (1+z) \frac{D(z, z_s)}{D_s} \int \frac{d^3k}{(2\pi)^3} \frac{\vec{k}_\perp}{k^2} \delta(k) \exp(-i\vec{k}_\perp \cdot \vec{x}_\perp(\vec{\theta}) - ik_r R) \quad (15)$$

---

<sup>2</sup>This expansion is not guaranteed to converge when the source is very near to a caustic, but if, roughly speaking,  $\mu_l\delta\kappa < 1$  this should not be a problem.

where  $\delta(k)$  is the Fourier transform of  $(\rho - \bar{\rho})/\bar{\rho}$ ,  $\rho_o$  is the current density of the universe and  $R$  is the radial distance. The correlation function for the deflection and any of its derivatives can be calculated with the Fourier version of Limber’s equation (Kaiser 1992) as is commonly done in weak lensing calculations. This is essentially the assumption that the quantities  $z$  and  $D(z)$  change less rapidly with  $R$  than  $\delta(\vec{x})$  does. The result is

$$\Delta\hat{\alpha}(\theta)^2 = \frac{4\pi}{H_o} \left( \frac{4G\rho_o}{D_s} \right)^2 \int_0^{z_s} dz \frac{(1+z)^2 D(z, z_s)^2}{\sqrt{\Omega_m(1+z)^3 + \Omega_\Lambda}} \int_0^\infty \frac{dk}{k} (1 - J_o[ky(z, \theta)]) P(k, z, M_{\max}) \quad (16)$$

where  $P(k, z)$  is the power spectrum of density fluctuations and  $J_o[x]$  is the zero-th order Bessel function. And by taking derivatives of (15), squaring and averaging, one can work out the variance of all the parts of the magnification matrix. Specifically

$$\sigma_\kappa^2(\theta) = \sigma_\gamma^2(\theta) = \frac{\rho_o^2}{2\pi H_o} \int_0^{z_s} dz \frac{(1+z)^2 \Sigma_{\text{crit}}(z, z_s)^{-2}}{\sqrt{\Omega_m(1+z)^3 + \Omega_\Lambda}} \int_0^\infty dk k J_o[ky(z, \theta)] P(k, z, M_{\max}). \quad (17)$$

The first equality comes from the fact that  $(k_1^2 - k_2^2)^2/4 + k_1^2 k_2^2 = (k_1^2 + k_2^2)^2/4 = k^4/4$ .

The power spectrum used here should really be a conditional power spectrum. As seen in equation (7), the deflection angle is proportional to the mass of the halo so the dispersion can be dominated by high mass halos. If no other galaxies are seen near the primary lens or they are included in the lens model for the primary lens then there is an upper halo mass (or light) cutoff,  $M_{\max}$ , implicit in this power spectrum. In practice,  $M_{\max}$  should be a function of  $z$  to express the detection limits of the observations.

#### 4. Discussion

It was demonstrated here that intergalactic matter is expected to cause changes in the magnification ratios that are of the same size as those that have been observed. This confirms, at least qualitatively, the conclusions derived from numerical simulations (Metcalf 2004). The possibility that the anomalies are from substructures inside the primary lens may not be consistent with  $\Lambda$ CDM (Mao et al. 2004; Amara et al. 2004), although simulations with high enough resolution to conclusively rule this out have not yet been done. Probably the best hope for distinguishing observationally between these two possibilities is to measure the dependence of magnification ratio anomalies on source redshift in a statistical way.

It was found here that the importance of intergalactic halos to the magnification ratios depends on the internal structure of the halos as well as the primordial power spectrum. The mass–concentration relation is of particular importance. This relation depends on the formation time of the halos (halos that form earlier are denser), the history of mass accretion and, in turn, on the slope of the primordial power spectrum and amount of dark energy. The concentrations could also change if the dark matter particle has a small mass (warm or tepid dark matter) or if it is self-interacting.

There are several factors that have not been taken into account here and would be expected to increase the importance of intergalactic structure. The halos will be strongly clustered which will clearly increase  $\sigma_\kappa$ . The scatter in the  $c$ - $M$  would be expected to increase halos’ influence on lensing as a population. The contraction of baryons within the halos will increase their concentration. Observed lenses (at a higher mass scale) have profiles closer to a SIS profile than the NFW profile. SIS halos will produce larger discrepancies in the magnifications. Finally,

intergalactic halos will have substructure of their own within them which will increase  $\sigma_\kappa$ . For these reasons the numbers given in this paper are conservative estimates.

To go beyond the variance in the image magnifications and to go beyond the unperturbed light path approximation numerical simulations are required. It has also been assumed here that the source is infinitely small which in many cases will not be a good approximation. One expects that when the size of the source is on the order of the size of the halos causing the lensing, the variations in the magnification will be smaller. Further simulations of specific lenses are needed.

Instead of thinking of this effect as lensing by individual galaxies in intergalactic space it might be better to think of it as a variation in the angular size distance as a function of position on the sky or a variation in the surface density of the universe. A typical line of sight travels through many halos (500 with  $10^7 M_\odot < M < 10^9 M_\odot$  for  $z_s = 3!$ ). On average they add up to the average surface density of the universe and the normal expression for the angular size distance calculated with the Robertson–Walker metric is recovered. However, there are variations in the surface density at the several percent level and these are enough to change the magnification ratios of multiply imaged quasars. This opens up an opportunity to probe the small scale, otherwise unobservable, structure in the universe which is shaped by the physics of the early universe as well as the history of star formation and reionization.

### Acknowledgments

I would like to thank J. Primack and R. Somerville for insight into the  $c$ - $M$  relation and M. Magliocchetti for helpful comments. Financial support was provided by NASA through Hubble Fellowship grant HF-01154.01-A awarded by the Space Telescope Science Institute, which is operated by the Association of Universities for Research in Astronomy, Inc., for NASA, under contract NAS 5-26555

### REFERENCES

- Amara, A., Metcalf, R. B., Cox, T. J., & Ostriker, J. P. 2004, preprint, astro-ph/0411587
- Bradač, M., Schneider, P., Steinmetz, M., Lombardi, M., King, L. J., & Porcas, R. 2002, *A&A*, 388, 373
- Bullock, J. S., Kolatt, T. S., Sigad, Y., Somerville, R. S., Kravtsov, A. V., Klypin, A. A., Primack, J. R., & Dekel, A. 2001, *MNRAS*, 321, 559
- Chen, J., Kravtsov, A. V., & Keeton, C. R. 2003, *ApJ*, 592, 24
- Chiba, M. 2002, *ApJ*, 565, 17
- Colín, P., Klypin, A., Valenzuela, O., & Gottlöber, S. 2004, *ApJ*, 612, 50
- Dalal, N. & Kochanek, C. S. 2002, *ApJ*, 572, 25
- Dekel, A. & Silk, J. 1986, *ApJ*, 303, 39
- Kaiser, N. 1992, *ApJ*, 388, 272
- Keeton, C. R. 2003, *ApJ*, 584, 664
- Kleyna, J., Wilkinson, M. I., Evans, N. W., Gilmore, G., & Frayn, C. 2002, *MNRAS*, 330, 792
- Mao, S., Jing, Y., Ostriker, J. P., & Weller, J. 2004, *ApJ*, 604, L5
- Mao, S. & Schneider, P. 1998, *MNRAS*, 295, 587
- Mateo, M. L. 1998, *ARA&A*, 36, 435
- Metcalf, R. 2004, accepted for publication in *ApJ*, astro-ph/0407298
- Metcalf, R. B. 2002, *ApJ*, 580, 696
- Metcalf, R. B. & Madau, P. 2001, *ApJ*, 563, 9
- Metcalf, R. B., Moustakas, L. A., Bunker, A. J., & Parry, I. R. 2004, *ApJ*, 607, 43

- Metcalf, R. B. & Zhao, H. 2002, *ApJ*, 567, L5
- Navarro, J. F., Frenk, C. S., & White, S. D. M. 1997, *ApJ*, 490, 493
- Press, W. H. & Schechter, P. 1974, *ApJ*, 187, 425
- Sheth, R. K. & Tormen, G. 2002, *MNRAS*, 329, 61
- Spergel, D. N., Verde, L., Peiris, H. V., Komatsu, E., Nolte, M. R., Bennett, C. L., Halpern, M., Hinshaw, G., et al., 2003, *ApJS*, 148, 175
- Treu, T. & Koopmans, L. V. E. 2004, *ApJ*, 611, 739